Chapter 3

Stability and Reliability of an Electrical Device Employing Highly Crystalline Single-Walled Carbon Nanotubes as a Field Emitter

Norihiro Shimoi

Additional information is available at the end of the chapter

http://dx.doi.org/10.5772/intechopen.72581

Abstract

Carbon nanomaterial is drawing keen interest from researchers as well as materials scientists. Carbon nanotubes (CNTs)—and their nanoscale needle shape—offering chemical stability, thermal conductivity, and mechanical strength exhibit unique properties as a quasi-one-dimensional material. Among the expected applications, field emission electron sources appear the most promising industrially and are approaching practical utilization. However, efforts to construct a field emission (FE) cathode with single-walled carbon nanotubes (SWCNTs) have so far only helped average out a non-homogeneous electron emitter plane with large FE current fluctuations and a short emission life-time because they failed to realize a stable emission current owing to crystal defects of the carbon network in CNTs. The utilization of CNTs to obtain an effective cathode, one with a stable emission and low FE current fluctuation, relies on the ability to disperse CNTs uniformly in liquid media. In particular, highly crystalline SWCNTs hold promise to obtain good stability and reliability. The author successfully manufactured highly crystalline SWCNTs-based FE lighting elements that exhibit stable electron emission, a long emission life-time, and low power consumption for electron emitters. This FE device employing highly crystalline SWCNTs has the potential for conserving energy through low power consumption in our habitats.

Keywords: single-walled carbon nanotube, high crystallization, field emission, wet coating process, thin film, scratch, planar light source, cathode luminescence

1. Introduction

The further development of electronic systems necessitates the production of efficient devices employing carbon nano-materials. Carbon nanotubes (CNTs) represent a promising material due to their unique physicochemical properties: their nanoscale needle shape, high chemical

stability, thermal conductivity, and mechanical strength. These properties confer an advantage in the fabrication of field emitters. The utilization of single-walled carbon nanotubes (SWCNTs) relies on their electronic properties since they can be either metallic or semiconductive, depending on the geometric configuration of a graphene sheet rolled up as a tube (i.e., diameter and chiral angle) [1–4].

CNTs express one-dimensional circumscription effects and have characteristics as quantum wires coherently [5–7], and CNTs have the highest Young's modulus of all known materials mechanically [8]. Owing to these outstanding properties, wide-ranging applications for nanotubes are currently under investigation, including their use as electron field emitters [9], probes in scanning-type microscopes [10], gas (e.g. hydrogen) storage materials [11], and as electrode materials for secondary batteries as well as in capacitors [12]. Among these proposed applications, field emission electron sources appear the most promising industrially and in fact are approaching practical utilization. When a highly electrical field in the order of 10^3 V/μm is applied onto a surface of an electron emitter, electrons emit from inside the emitter's solid to a vacuum atmosphere by the quantum-mechanical tunneling effect. This phenomenon is called the field emission. Such an extremely high field can be obtained on the sharp tip having a thin needle because electric fields concentrate at the top of the sharp tip. It is said that the carbon nanotubes possess the following physical or chemical properties for field emitters: 1) a high aspect ratio with a sharp tip, 2) high mechanical strength, and 3) high chemical stability. Field emission (FE) phenomenon from an isolated single multiwalled carbon nanotube (MWCNT) was first reported by Rinzler et al. [13] in 1995, and FE from a MWCNT film was reported by de Heer et al. that same year [14]. Subsequently, many experimental studies on FE from MWCNTs [15–18] and SWCNTs [19] have appeared. Field emission microscopy (FEM) has also been used to clarify the geometric structures of the nanotube tips [16, 19]. Moreover, many studies have attempted to employ CNTs as field emitters in a display cathode with a lower driving voltage and stable electron emission. These trials mostly involve the vertical alignment of the CNTs in their fabrication that are synthesized by plasma-enhanced chemical vapor deposition (PECVD) or laser abrasion fabrication; for example, screen printing with high-viscosity submicron to micron scale metal-particle paste to fabricate patterned field emitters has been proposed [20–22]. However, these approaches could not obtain the homogeneous electron emitter plane with small FE current fluctuations as they failed to construct a uniform thin film employing a homogeneous dispersion of CNTs.

The utilization of CNTs to obtain an effective cathode—with both a stable field emission and low FE current fluctuation—hinges on the ability to disperse them uniformly in liquid media. In particular, highly crystalline SWCNTs can be expected to emit electrons stably with a low turn-on and driving voltage, yet their homogeneous dispersion has yet to be reported. For this study, we selected a low-viscosity solvent with an In_2O_3-SnO_2 (tin-doped indium oxide; ITO) precursor solution as the conductive matrix material being dispersed highly crystalline SWCNTs. A dispersant was added to obtain the well-dispersed highly crystalline SWCNTs, and the mixture with the ITO solvent, highly crystalline SWCNTs, and the dispersant was agitated by an ultra-sonic homogenizer.

This chapter first briefly reviews the synthesis of highly crystalline SWCNTs by arc discharge and their structural characterization [23], followed by a discussion of the characteristic properties

of FE from the arc-produced nanotubes, concluding with a description of the application of the nanotube emitters in a flat-panel lighting device. Here, the author successfully manufactured SWCNT-based field emission lighting elements exhibiting stable electron emission, adequate luminance, and low power consumption for the electron emitters.

2. Experimental crystallization of annealed SWCNTs

Purified and highly crystalline SWCNTs synthesized by arcing and sintered at high temperature in a vacuum have been expected to serve as an electrical source material for a field emitter though the homogeneous dispersion of highly crystalline SWCNTs has yet to be reported. This is because highly crystalline SWCNTs have almost no defects in the carbon network on their surface, nor do they combine with another functional group of dispersants. It is difficult for SWCNTs aggregated as a secondary particle to separate uniformly into single nanotubes. Furthermore, despite the necessity of a thin film homogeneously dispersing highly crystalline SWCNTs for a field emission cathode plate, as yet no method for synthesizing a thin film with SWCNTs for a field emitter exhibiting a good homogeneity of plane-light emission has been developed.

In this chapter, commercial arc-SWCNTs (ASP-100F, Hanwha Chemicals Co. Ltd., Korea) were used. The SWCNTs were annealed at a high temperature (around 1000 K) in a high vacuum (pressure, $>10^{-5}$ Pa) to obtain highly crystalline SWCNTs. **Figure 1** shows transmission electron microscopy (TEM, HR-3000, Hitachi High-Technologies Corporation, Japan) images of the SWCNTs (a) after and (b) before annealing as a reference. As shown in **Figure 1(a)**, the crystallinity of the SWCNTs was significantly improved after annealing at a high temperature in a tight vacuum.

Here, analytical grade reagents were used in the experiments. The annealed arc-SWCNTs checked for high crystallization were measured by Raman-shift. The Raman spectrum measured by the blue laser beam (Blue) at a 473 nm wavelength is shown in **Figure 2**. Raman peaks from the G+ band mode (1590 cm^{-1}) and from the G_ band mode (1565 cm^{-1}) presumed to be nanotube structures. A Raman peak intensity of near 1350 cm^{-1} from the D band mode indicated lacks of carbon network on a nanotube. The intensity ratio between the G+ band and the D band was 0.0096; this value confirms that the SWCNT has a carbon network with high crystallization.

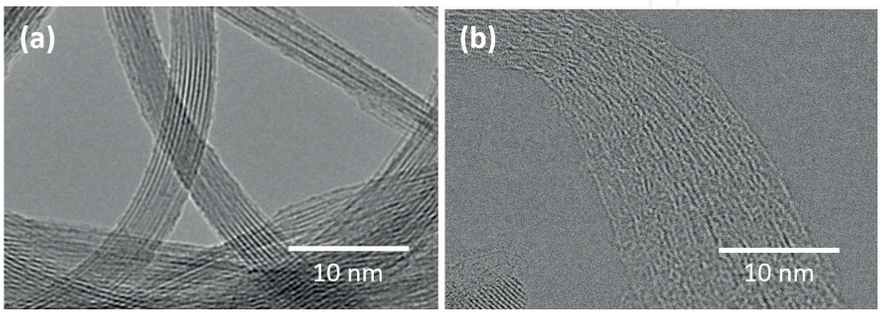

Figure 1. TEM images with annealed and unannealed SWCNTs [24]. (a) Highly crystalline SWCNTs with annealing treatment. (b) SWCNTs with crystal defects without annealing treatment.

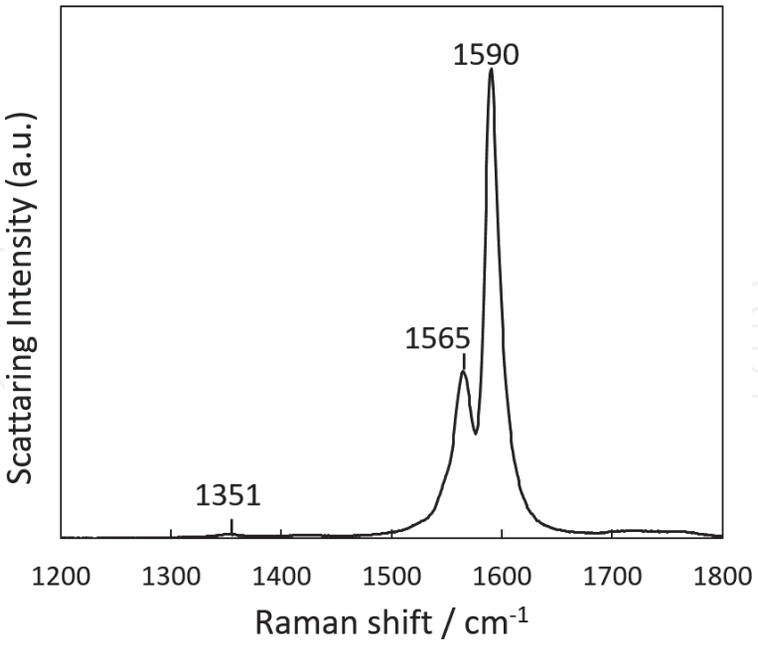

Figure 2. Raman spectrum with G and D band modes of annealed SWCNTs. [25].

3. Construction of a thin film including highly crystalline SWCNTs for field emission

A wet-coating process was adopted to fabricate a cathode with stable FE at a low driving voltage using SWCNTs. The homogeneous dispersion of SWCNTs in a liquid medium was the key. Highly crystalline SWCNTs are expected to lower the threshold field and emit electrons stably at a low driving voltage, but no homogeneous dispersion of SWCNTs in liquids has ever been reported. In general, a dispersant is used to facilitate the homogeneous dispersion of nano-carbon materials in liquids; however, highly crystalline SWCNTs cannot bind to the functional groups in a dispersant because there are very few defective binding sites in their carbon network that can be used to bind to these in the dispersant. We attempted to separate highly crystalline SWCNT aggregates physically into uniform single nanotubes in a low-viscosity solvent containing an In_2O_3-SnO_2 (tin-doped indium oxide; ITO) precursor solution. A nonionic dispersant was added to the solvent to facilitate the dispersion of SWCNTs, and the mixture was agitated with ceramic beads in a shaking machine.

The physical properties for producing a mixture including highly dispersant SWCNTs are as follows: Butyl acetate 99%, ethyl cellulose (EC) (abt. 49% ethoxy 100 cP), and sodium *linear*-alkyl-benzenesulfonate 95% (DBS) were obtained from Wako Co. Ltd. Japan. The initial mixture was prepared by mixing the SWCNTs powder with the ITO precursor from Kojundo-Kagaku Co. Ltd. Japan and the DBS and the EC in a proportion of about 1: 600: 1: 4. The last component, EC, was tried in different proportions. The mixture was later agitated with ZrO_2 beads of different diameters in various concentrations from 4 g to 8 g in a shaking machine at periods ranging from 6 h up to 12 h. In all cases, the resulting mixture solution shown in **Figure 3** had low viscosity. The TEMs of the annealed SWCNTs are shown in **Figure 3**; almost only carbon nanotubes can be seen in the micrographs, with no other carbon contamination present.

http://dx.doi.org/10.5772/intechopen.72581

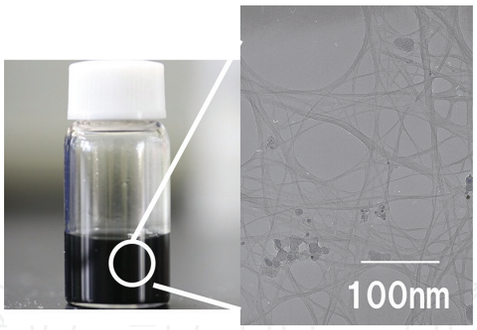

Figure 3. Dispersed SWCNTs mixture and TEM observation [25].

In order to confirm the crystallinity of SWCNTs, the TG first derivative (dTG) curves for both of the annealed SWCNTs and non-annealed samples presented in **Figure 4** indicate the weight fraction of tubes at each burning temperature. It is generally known that the burning temperature of SWCNTs is inversely proportional to the amount of crystal defects in the SWCNTs; hence, the SWCNT crystallinity can be inferred from the shape of the dTG curves. There are a few peaks in the non-annealed SWCNT dTG curve, indicating a range of different crystallinities; the burning temperature of the SWCNTs increased after annealing, signaling an increase in the degree of crystallinity of the SWCNTs. However, the non-annealed SWCNT dTG curve also indicated the presence of some lower crystallinity tubes that might affect the field-emission stability.

The relationship between dispersion concentration and crystallinity retention rate for highly crystalline SWCNT dispersions prepared by ultra-sonication and agitation with ceramic beads is shown in **Figure 4**. The dispersion concentration in **Figure 5** was calculated from the ratio of dispersion transparency before and after centrifugation of the solution, as determined by UV–vis measurements, and includes highly crystalline SWCNT aggregates. The crystallinity retention was calculated from the dot product of dTG measurement curves obtained before and after dispersion of the highly crystalline SWCNTs and is presented as cosθ. A reduction in cosθ correlates to a deterioration in the crystallinity of the dispersed highly crystalline SWCNTs. Thus, **Figure 5** indicates that the SWCNT crystallinity deteriorates with

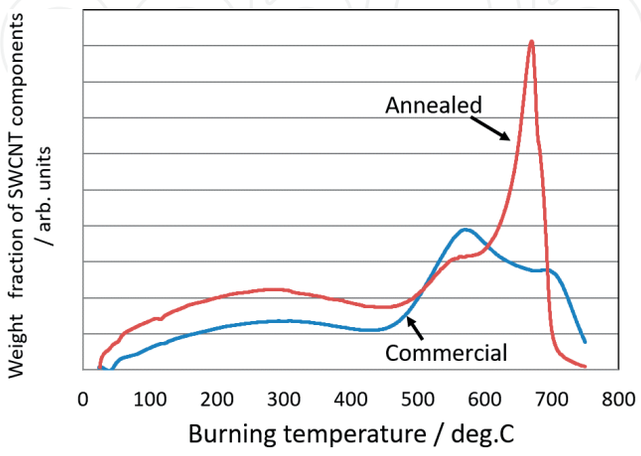

Figure 4. First derivative thermogravimetric curves of the commercial and annealed single-walled carbon nanotubes measured under an air atmosphere.

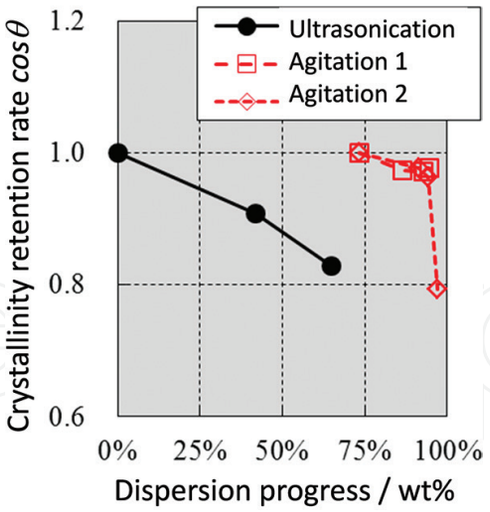

Figure 5. Dispersion concentration vs. crystallinity retention rate for highly crystalline single-walled carbon nanotubes dispersed by ultra-sonication and agitation. Ultra-sonication at 40 kHz was performed for 0, 5, and 10 hours. Agitation was carried out under different conditions and repeated several times.

increasing sonication time; we presume this to be an effect of the uncontrollable cavitation that occurs during ultra-sonication. The agitation method was the most successful method for highly crystalline SWCNT dispersion, with a concentration of more than 90 wt% and minimal crystallinity deterioration achieved. However, it should be noted that the crystallinity of the dispersed highly crystalline SWCNTs also deteriorates with repeated milling and at higher operation pressures. This is likely owing to a difference in atom binding energy and cohesion energy depending on the higher-order structure of SWCNTs [25, 26].

In this chapter attempts were made to disperse SWCNTs with a low-viscosity butyl acetate solvent including an organic In_2O_3-SnO_2 (ITO) precursor and non-ionic dispersant. The author successfully employed a dispersion method for highly crystalline SWCNTs to obtain a mixture of them dispersed as thin bundles, aggregating with a few nanotubes. The agitated mixture was sprayed onto a metal-coated glass substrate heated to around 400 K, and the coated film was sintered at 900 K in a vacuum to remove any organic components and then form bridges in order to produce a conductive ITO film. After a film coated with the mixture was sintered in a vacuum, it was activated by scratching it appropriately to obtain field emission properties with a low turn-on field. **Figure 6** shows SEM images of an ITO film with dispersed SWCNTs after vacuum sintering. The ITO film was scratched by a thin metal rod; this revealed SWCNTs or their bundles protruding from both sides of the edge of the ITO film. As shown in **Figure 6(a)**, highly crystalline SWCNT bundles were dispersed. As shown in **Figures 6(b)** and **6(c)**, the SWCNT bundles were exposed in the scratched grooves on the ITO film subjected to activation treatment. The white circles in the SEM image of **Figure 6(a)** indicate the exposed SWCNT bundles that were exposed by scratching the ITO film in which SWCNTs were dispersed. White circles show the distances between their points to be almost identically aligned. SWCNTs in the ITO film were dispersed homogeneously and lay in random directions. Thus, SWCNTs would appear in same direction in the ITO film with the same probability, and homogeneously dispersed SWCNTs protruding from the grooved face of the ITO film could be observed.

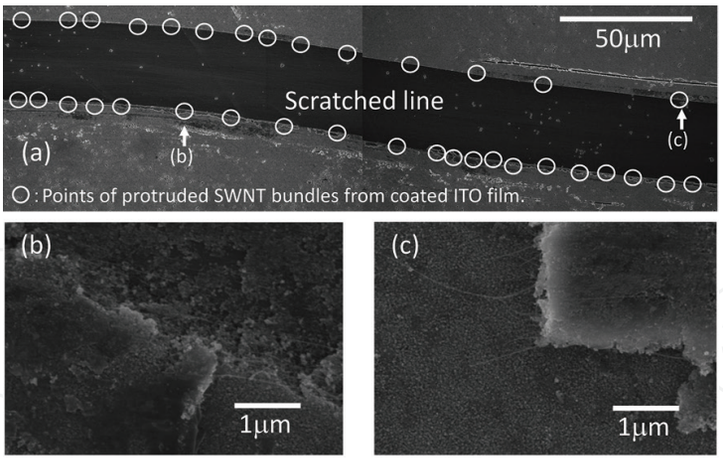

Figure 6. SEM images of ITO film with dispersant SWCNTs after sintering [25]. (a) Overview of a scratched ITO film. White circles indicate points of SWCNT bundles protruding from the ITO film as measured by SEM. (b) and (c) enlarged images arrowed in the image of (a). The white arrows indicates SWCNTs from the grooved face.

In this chapter, the SWCNTs coating weights per unit area were controlled by the numbers of spray cycles to verify both the field emission property and brightness efficiency of a flat-plane light emission panel. The sintered film was fabricated using an activation process without the standing or aligning treatment of the CNTs in order to emit electrons easily at low voltage.

Then the SWCNTs for the field emitter protruding from the grooved face were aligned in a direction parallel to the ITO film plane and substrate per the schematic drawing in **Figure 7**, which shows schematic drawings of the models with random directions for the SWCNTs. The dotted square boxes indicate scratched areas, and the tops of SWCNTs that possibly emit electrons are highlighted with red circles in the area. These depend on the density of the SWCNTs in a coated film. The direction of the SWCNTs exposed by scratching aligns in a direction parallel to the substrate, so electrical fields are yielded at the top of each SWCNT uniformly without the fluctuation of the protruding SWCNT length. We thus obtained high homogeneity for the electron plane-emission with the dispersion and density of SWCNTs in the coated film.

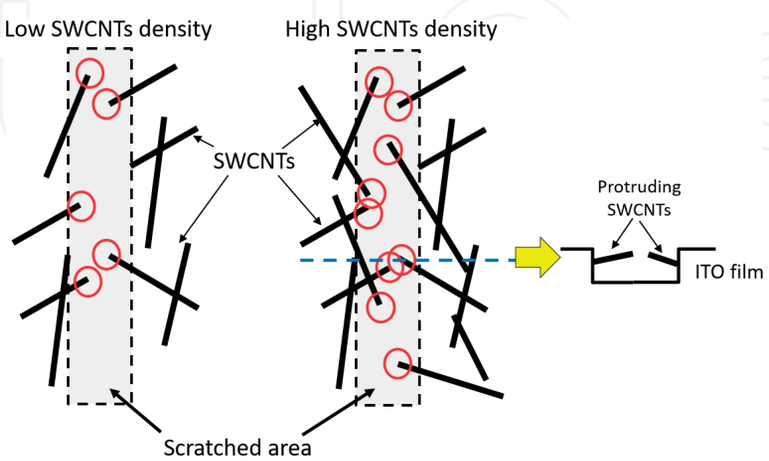

Figure 7. Images of frequency in the exposure of SWCNTs in a scratched area in cases of both low and high SWCNT density. Red circles indicate the exposed tops of SWCNTs. [25].

4. Field emission properties

This activated field emission (FE) cathode employing highly crystalline SWCNTs has the potential to yield a new flat-plane light emission device and so provide a novel approach to daily lighting needs while also contributing to energy-saving through its low power consumption. FE properties were measured with a phosphor anode plate on a sputtered ITO pattern film and 1.0 millimeter glass plate as a spacer as shown in **Figure 8**.

The sample shown in **Figure 8** was set into the electrical circuit in **Figure 9** to measure field emission and brightness properties. This measurement system was constructed with a power supply unit having an amplifier, a function generator, an oscilloscope as a field emission current monitor, and a PC for data storage. The voltage for the sample was designed for a periodic voltage at 60 Hz of the triangle wave for field emission measurements. The field emission current was converted to bias voltage data by a resistor at around 10 to 1 MΩ for the purpose of preventing signal noise from any leaking current appearing in measurement applications.

The author attempted to control field emission characteristics by the weight of the SWCNTs included in a coated ITO film with activation by a simple scratching. **Figure 10** shows the current density-electrical field characteristics of the cathode with a 20 x 20 mm diode depending on the content of the SWCNTs in the coating film. For example, the contents for measurements were chosen at 1.07, 0.69, 0.35, and 0.09 mg/cm^2. The turn-on field increased as the SWCNT density rose to around 0.8 to 1.7 V/μm. The high SWCNT density obtained a low driving supply because of the increase in the field emission site available to emit electrons from the tip of each SWCNT.

The F-N electron tunneling function has been proposed as follows [27]:

$$I = a * V^2 * \exp\left(-\frac{b}{V}\right) \tag{1}$$

where

$$a = \alpha * A * \beta^2 * \exp\left(\frac{B * 1.44E-7}{\phi^{0.5}}\right)/(1.1 * \phi) \tag{2}$$

$$b = \frac{0.95 * B * \phi^{3/2}}{\beta} \tag{3}$$

$$A = 1.54E-6, B = 6.87E+7 \tag{4}$$

From Eq. (1), V means a voltage added between two electrodes; this is converted to an electrical field by the gap of the measurement sample in **Figure 8**. I indicates a current flow passing through the phosphor plate in the anode area at 20 × 20 mm^2. α is equivalent to the electron emission site area for the field emission based on Fowler-Nordheim tunneling, β is the field enhancement factor of the electrical field localized at the top of a SWCNT against a macroscopic applied electric field, and ϕ of 4.7 eV is the work function in the bulk region of carbon materials. **Figure 11** shows the distributions of α and β converted from the current density-electrical field characteristics by Eqs. (1), (2), (3) and (4) against the SWCNT coating density.

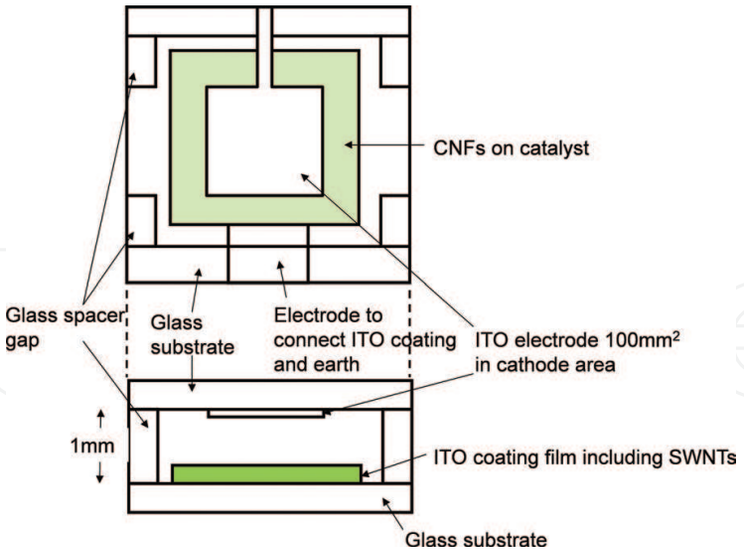

Figure 8. Schematic diagram of the system for FE measurement having a diode structure [25].

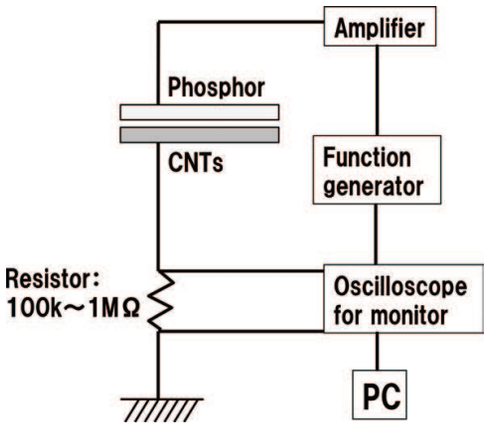

Figure 9. Schematic diagram of the electrical circuit system for FE measurement with a diode structure [25].

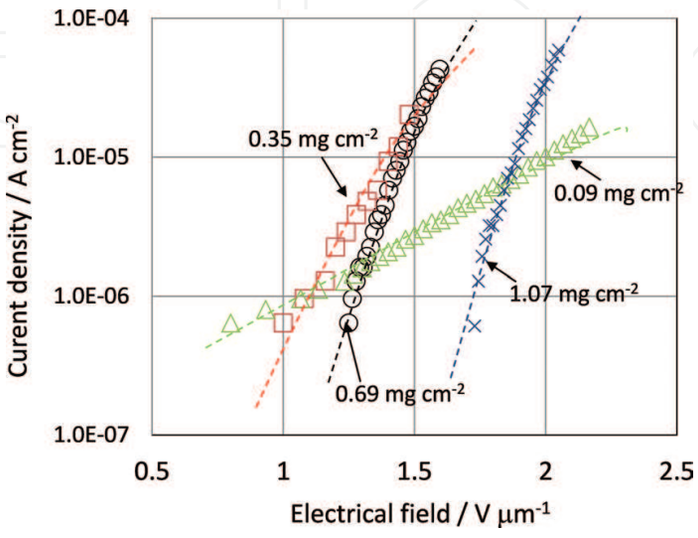

Figure 10. Current density-electrical field characteristics of certain conditions: 0.09, 0.35, 0.69, and 1.07 mg/cm² [25].

The flat emission-plane—especially for the content of SWCNTs at 0.69 mg/cm^2—from the diode generated a stable, homogeneous brightness of over 2000 cd/m^2 in the sampling area of 400 mm^2 without any brightness fluctuation. The brightness of the sample with the content of SWCNTs at 0.69 mg/cm^2 was measured at nine locations in the emission area, as captured by a charge coupled device (CCD) camera in **Figure 12**. Furthermore, the differences between each brightness result of the measurement points in the plane shown in **Figure 8** were within 5% of those shown in **Figure 13**; accordingly, stable brightness uniformity was achieved in the plane-emission area.

$$Brightness\ \ Efficiency(lm/W) = \frac{Brightness(cd/m^2) \times Lighting\ area(m^2) \times 3.14}{Voltage \times 0.5 \times FE\ \ Current \times \exp(-2.4)} \quad (5)$$

As calculated by the luminance measured by a luminance meter and the load power compensated as a direct current (DC) load power for the effective voltage of the triangle wave—indicated as *Voltage* × *0.5* in Eq. (5)—as a bias voltage and effective field emission current, which was indicated as *FE Current* × *exp.(−2.4)* in Eq. (5), the author was able to achieve a brightness efficiency calculated by Eq. (5) of more than 70 lm/W within an area of approximately 25 cd/m^2 of brightness standard deviation by controlling the contents of SWCNTs in the coated film. Phosphor plates for brightness efficiency measurements were chosen for their green lighting from Nichia-Kagaku Co. Japan. The green circular points in **Figure 14** indicate the brightness efficiency with a green phosphor emitting light. The square blue points represent the deviation of brightness employing the green light in the plane-emission area shown in **Figure 12**. The brightness properties from the developed cathode depended on the content of the SWCNTs and could be obtained with high brightness homogeneity and high driving efficiency by controlling the SWCNT density in the coated ITO film. However, the brightness efficiency in case of a SWCNT density of more than 0.69 mg/cm^2 decreased with an increase in the SWCNT density from **Figure 14**. This is probably owing to the electrical field strength for field emission focused on each top of the SWCNTs being weaker than 0.69 mg/cm^2; though SWCNTs as electron emission sites are sufficient for obtaining a high field emission current. This can be explained by the tendency of the field enhancement factor in **Figure 11**, which causes the distance between neighboring SWCNTs as field emitters to narrow with the increase in SWCNTs density. Moreover, the tendency of the brightness deviation is for a stability of more than around 0.69 mg/cm^2. Most likely, this is because enough SWCNTs for field emitters exist in the ITO film for a high SWCNT density. From **Figure 14**, it is apparent that a high brightness efficiency could be obtained by controlling the SWCNTs density in the ITO film. To our knowledge, this is the first time a field emitter plane device has achieved a high brightness efficiency of over 70 lm/W.

Figure 15 shows the field emission life time up to 100 hours at SWCNT contents of 0.09, 0.35, and 0.69 mg/cm^2. FE-current was measured as a peak of field emission current with a periodic voltage of the rectangular wave with a frequency of 60 Hz and duty ratio of 10%, and initial FE-current density was adjusted approximately to 45 mA/ cm^2. This result implies that the radioactive half-time will be over 5000 hours at 0.69 mg/cm^2, and other samples with a SWCNT density of more than 0.69 mg/cm^2 have the same emission-life tendency as at 0.69 mg/cm^2. Attenuation of the loading field emission current depends on the uniformity of the loading power, equal to the electrical field strength, given to each SWCNT for field emitters. A field emitter-plane employing SWCNTs will have the high stability with a high crystallization of

http://dx.doi.org/10.5772/intechopen.72581

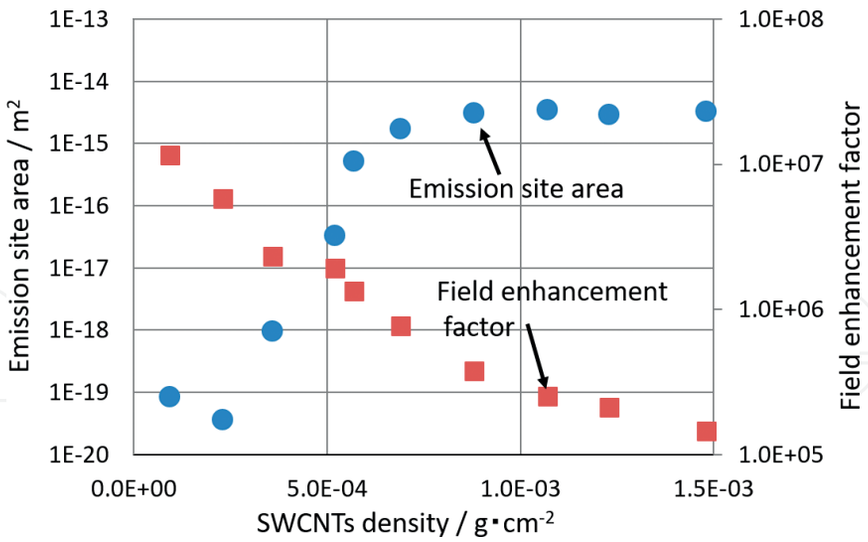

Figure 11. The dependence between the emission site area, field enhancement factor, and SWCNT density [25].

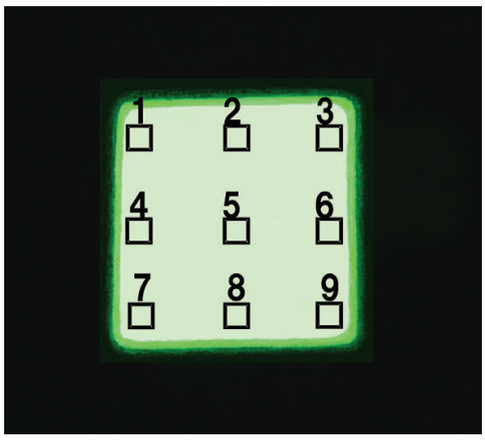

Figure 12. Light emission brightness image of the SWCNT content 0.69 mg/cm² among nine areas captured by CCD through a ND filter. The added voltage between the anode and cathode is 3.0 kV with a peak-to-peak range of periodic voltage in the triangle wave; the flow current is 250 μA as a peak currentw [25].

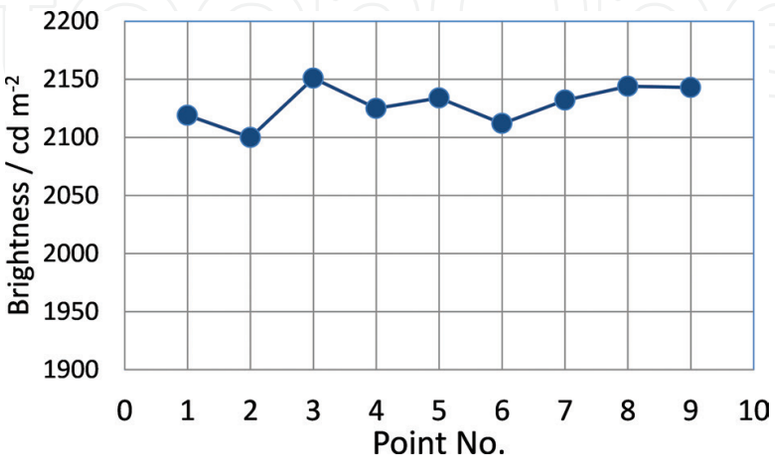

Figure 13. Brightness results at the points of flat light emission in **Figure 12** [25].

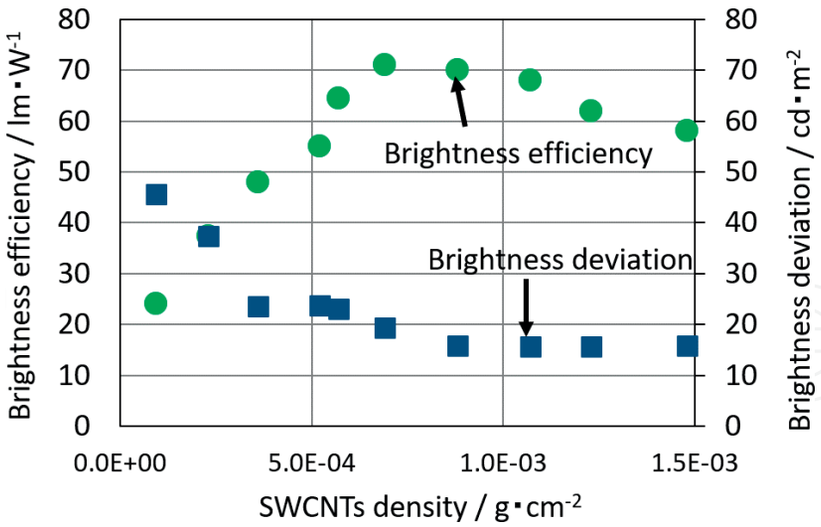

Figure 14. SWCNT content density with the dependence of brightness efficiency indicated on the left vertical axis and brightness homogeneity on the right vertical axis. The peak-to-peak voltage condition of the triangle wave is fixed at 5 kV [25].

the SWCNTs and high emission site homogeneity from **Figures 11** and **14**, and it will obtain a long emission life-time to withstand practical use as a plane-light emitting device. The coated, highly crystalline SWCNT cathode has potential for realizing a visible ray flat plane-emission device with low power consumption and a long product life cycle.

Figure 16 shows the distance distribution between neighboring SWCNTs depending on the SWCNT density. The results were measured from the total number of SWCNTs protruding from the groove face of an arbitrarily scratched ITO film by visual observation with an SEM image, as that in **Figure 7**. SWCNTs were exposed from the side wall of the grooved face into the ITO film. The distance between SWCNTs protruding from the grooved face depends on

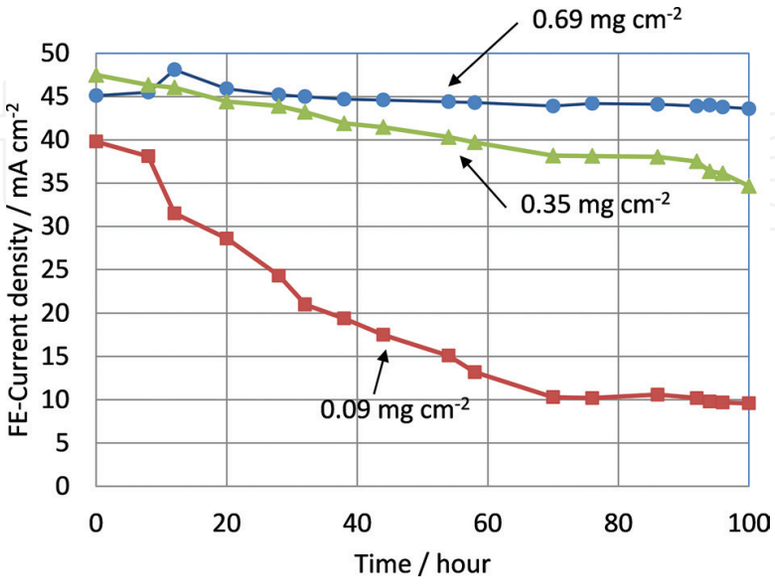

Figure 15. The lifetime of field emission current density up to 100 hours. The half time against the initial field emission current density of 0.69 mg/cm^2 will be over 5000 hours [25].

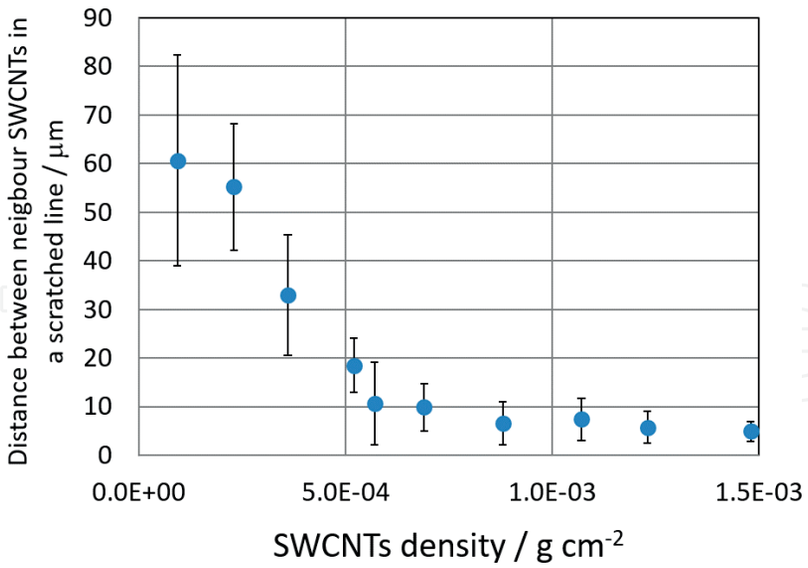

Figure 16. The dependence on the distance between neighboring SWCNTs protruding from the edges of ITO film and SWCNT density [25].

the SWCNTs density; it averages approximately 10 μm at 0.69 mg/cm^2. If SWCNTs are well dispersed in the ITO film and align randomly, their protrusions aligning along a direction in the groove made by a voluntary scratching process appear uniform. The protruding SWCNT length measured by SEM was generally 4–6 μm. The ratio of the average distance and length of SWCNTs via SEM images was nearly 2, and it is believed that the electrical field to obtain a high field emission current is added at the top of each protruding SWCNT of 0.69 mg/cm^2 [28]. Then the SWCNTs for the field emitter protruding from the grooved face were aligned in a direction parallel to the ITO film plane and substrate as shown in **Figure 6** and the schematic drawing in **Figure 7**, which shows such drawings of the models with random directions for the SWCNTs. The dotted square boxes indicate scratched areas, and the tops of SWCNTs that possibly emit electrons are highlighted with red circles in them. These depend on the density of the SWCNTs in a coated film. The direction of the SWCNTs exposed by scratching aligns in a direction parallel to the substrate, thereby uniformly yielding electrical fields at the top of each SWCNT without any fluctuation of the protruding SWCNT length. We thus obtained high homogeneity of the electron plane-emission with the dispersion and density of SWCNTs in the coated film.

The flat plane-emission from the simple diode panel generated a stable and homogeneous brightness of over 2000 cd/m^2 in the sampling area as shown in **Figure 12** without current fluctuation in the plane. The current fluctuation of emissions from the flat plane panel with an added voltage of 4 kV DC was stable over a period of 150 minutes as shown in **Figure 17**. This degree of electron emission stability is excellent for highly purified and crystallized SWCNTs in a diode panel. In particular, highly crystallized SWCNTs have no defects in their carbon network [23, 29], and such perfect crystallization prevents SWCNTs from breaking down with a large field emission current. Previously, it was necessary for a stable field emission current by CNTs with low power consumption to construct the triode structure, to synthesize carbon nanotubes designed with vertical alignment and standing height uniformly on an electrode by CVD with high temperature, and to obtain a high vacuum atmosphere around over 10^{-6} Pa in a panel [30]. In this study, we were able to obtain a stable large field emission current in a simple diode panel for the first time ever.

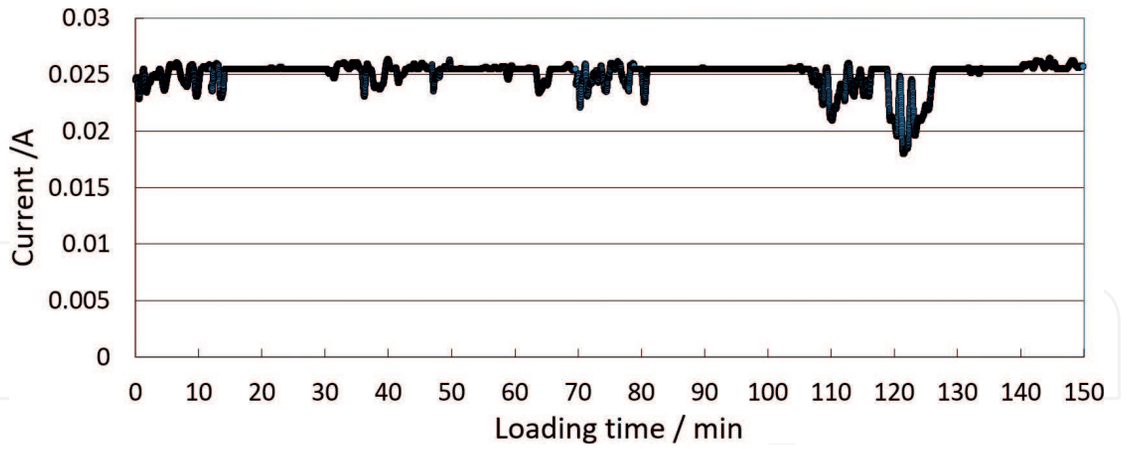

Figure 17. Current fluctuation with 4kVDC loading for 150 minutes [31].

5. Basic design of the triode structure

The following time, a triode structure employing highly crystalline SWCNTs was attempted to serve as a prototype device of a flat-panel illumination shown in **Figure 18**. This device had a cathodoluminescence structure and had three electrodes for the FE electron emissions as a cathode, the switching of FE electron emissions on and off as a gate, and the radiation of visible rays by electron impact as an anode electrode. The cathode and the gate electrode, which apply voltage sequentially (called as line sequential scanning method) for electron emissions from the cathodes respectively, were patterned along the same line referred to **Figure 18**. Furthermore, a mixture of the long afterglow phosphor (P-1 from Mitsubishi Chemical) material with fluorescent material (P-22 from Nichia) that conducts a high luminance output was used for the anode electrode.

A stripe patterned structure was adopted for the gate electrodes used for on/off switching of the FE electrons, as shown in **Figure 18**. An FE electron emission site existed at the edges of

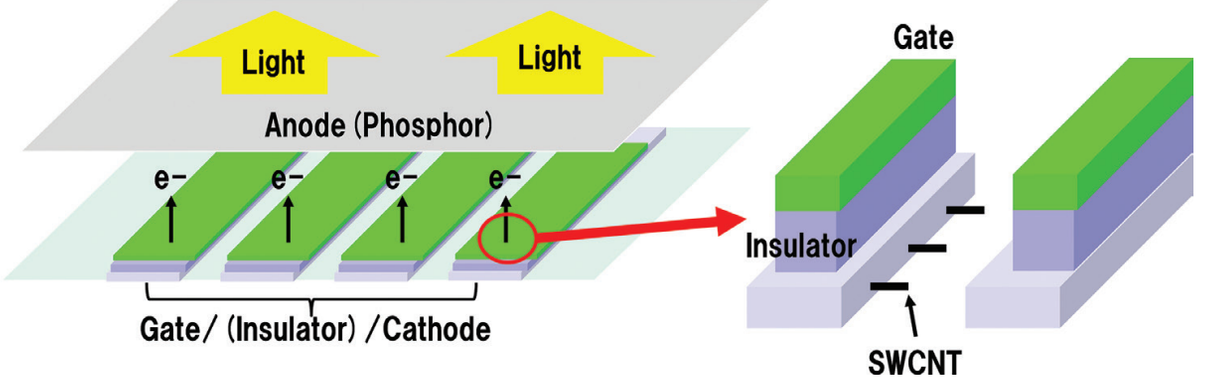

Figure 18. Basic structure of the triode flat-panel light-emission device [32]. Copyright (2017) The Japan Society of Applied Physics.

the tops of the SWCNTs, exposed on the both sides of the nicks scraped on the coating by a picking tool [25]. Thus, no exposed SWCNT was raised for field emission of electrons. The edges of the SWCNTs, as well as the width of the stripe patterned gate electrodes referred to **Figure 18**, were designed in an attempt to minimize the driving voltage for on/off switching of the FE electrons. In relation to the field intensity at the edges of the tops of the SWCNTs exposed on the both sides of the nick in **Figure 18**, the electrical potential distribution in the space, along with the electrode width dependence of electrical potential distribution at the edges of the SWCNTs, were simulated according to the surface charge method [33–36].

The cathode electrodes were grounded stationary while the anode electrode applied a direct-current (DC) voltage. The acceleration conditions for the electrons irradiated on the phosphor were taken into consideration to obtain a high brightness efficiency within a few kilo-volts. Conditions to apply electrical potential to emit FE electrons were controlled for the gate electrodes because the FE electrons were emitted at constant field intensity.

The length of the SWCNTs protruded from the wall, the width of the nicks made using a picking tool and the aperture of the stripe patterned electrodes of the gate electrodes were designed at 1 μm, 30 μm, and 40 μm, respectively. This was done to change the voltage applied to the gate electrodes to the negative direction in order to transit of electrical potential. A schematic diagram of the calculation model, as well as the calculation results, is shown in **Figure 19**.

The electrical potential along the z-axis in cases where the voltage applied to the gate electrodes set at 0, −1, −3, and −5 V was calculated. The z-axis was defined as the direction extended from the origin located above the edge of the SWCNT where electrons are emitted. The potential distribution depended on the voltage applied to the gate electrode. It was determined that the threshold voltage of the FE electron emissions was reached at a voltage of approximately −3 V applied to the gates of the corresponding model. We attempted to fabricate a prototype device of a triode planar light-emitting device based on the above calculation results.

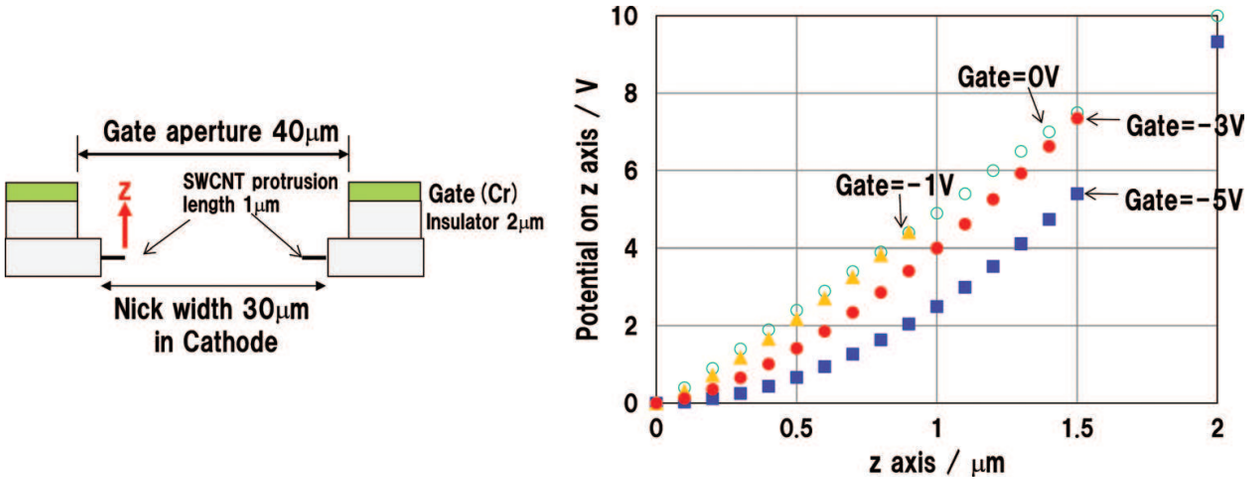

Figure 19. Schematic diagram of (left) calculation model and (right) calculation results [32]. Copyright (2017) The Japan Society of Applied Physics.

6. Correlation between driving power and light-emitting characteristics of a light-emission device

The prototype trial pattern for a triode-structure planar light-emission device is shown in **Figure 20**. Thin silicon oxidation film as an insulation layer was formed on a silicon wafer by using thermal oxidation treatment to assemble cathode, insulator and gate electrodes. The electrodes were laminated outward nearest the silicon oxide film by using the SWCNTs within an ITO film for the cathode electrode, a silicon oxide film of 1-μm thickness (formed using the TEOS-CVD method) as an insulation film, and a thin chrome film as a gate electrode. Gate electrodes, insulation films and cathodic electrodes installed SWCNTs were designed in a stripe pattern at the FE electron emission area as shown in **Figure 20**. The cathode electrodes between the gate electrodes were scratched in a line using a picking tool to expose and protrude the SWCNTs as FE emitters. The light-emitting area was designed to have an area of 15 × 15 mm^2.

Electron leakage at the gate electrodes was verified when electrons were emitted from the SWCNTs. The cathode and gate electrodes were installed on the ground. The spectra detected at the both electrodes being applied a pulse voltage is expressed in **Figure 21**. The voltage applied to the anode electrode by blue solid line and the current flowing through the cathode and gate electrodes are respectively represented by solid lines of red and gray. Almost no current was flowing through the gate electrode, while the FE current loading between the cathode and anode electrodes was confirmed.

A pulsed voltage was applied to the gate electrode, and a waveform was prepared to apply negative voltage by adding an offset voltage as a pulse signal. The system was driven by an operation mechanism to cut off the FE current, and it timed with the application of a few volts at the gate in the negative direction. A schematic diagram of the loading system for the prototype trial pattern for a triode-structure planar light-emission device is shown in **Figure 22**.

Conditions of the light emission, when switching on/off of the gate electrode, are shown in **Figure 23**. A stable FE current flowed between the cathode and anode electrodes when the voltage on the gate was 0 V. However, when a voltage of −3 V was applied to the gate electrode, we could find no current was flowing between the cathode and anode electrodes. These results of lighting emission indicated a successful control of the on-and-off switching of the current by switching gate electrodes.

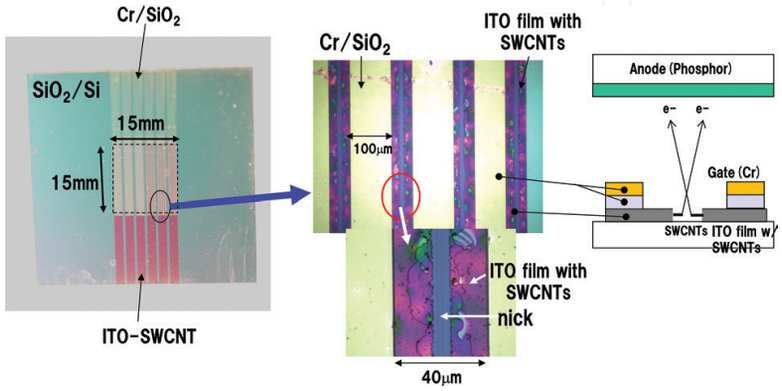

Figure 20. Prototype trial pattern of cathode gate electrode structure [32]. Copyright (2017) The Japan Society of Applied Physics.

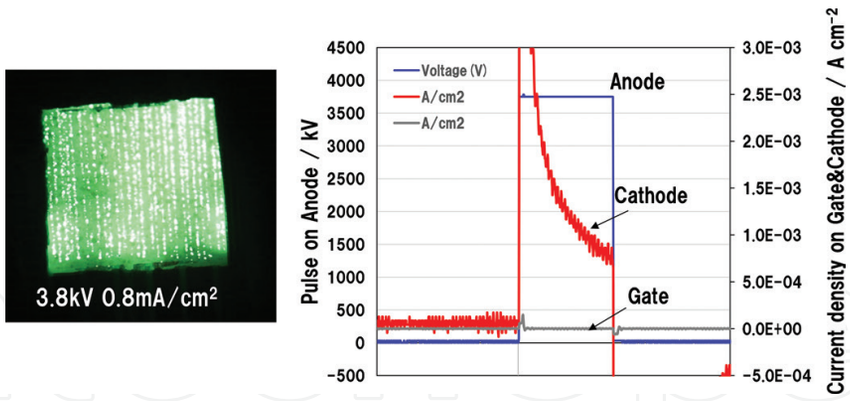

Figure 21. Cathode and gate-anode electrodes: Synchrony of a leaked current flowing through cathode and gate electrodes with signals of voltage applied to the anode, and depiction of a leaked current flowing through gate electrode [32]. Copyright (2017) The Japan Society of Applied Physics.

A mixed powder with the long-afterglow-type (P-1) and the high-luminance-output-type (P-22) phosphors was employed as a fluorescent material for the line scanning sequential test. The weight ratio of the mixture was designed to obtain the highest brightness efficiency. The frame scanning frequency was 60 Hz. A sequential timing chart to apply voltage to the gate electrodes on the six electrode lines of the prototype device was adopted for our development. We developed a scanning algorithm to amplify the light-emission luminance by overlapping the afterglow component of the long-afterglow-type phosphor with the high-luminance-output fluorescent material component of the subsequent frame scanning.

The FE current value flowing throughout the device and the luminance output from the anode were controlled by the voltage applied to the gate electrodes. The correlation between the energy power consumption and the luminance output by driving the device is shown in **Figure 24** from the results of light-emission evaluations. We could succeed to obtain a high luminance output of over 12,000 cd/m^2 and higher with a power consumption of approximately 0.1 W during driving the test panel. This outcome indicates that we were able to derive the higher performance in the world for a flat-panel light-emission device by achieving a brightness efficiency of 87 lm/W.

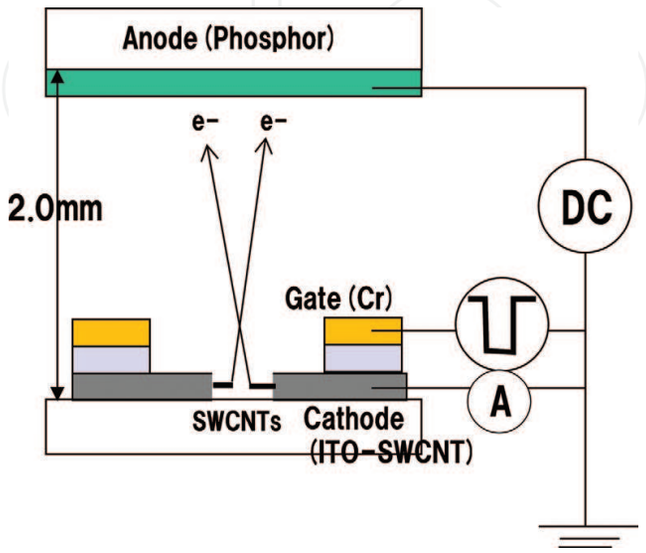

Figure 22. Schematic diagram of electrode wire connections and electrical circuit for drive [32]. Copyright (2017) The Japan Society of Applied Physics.

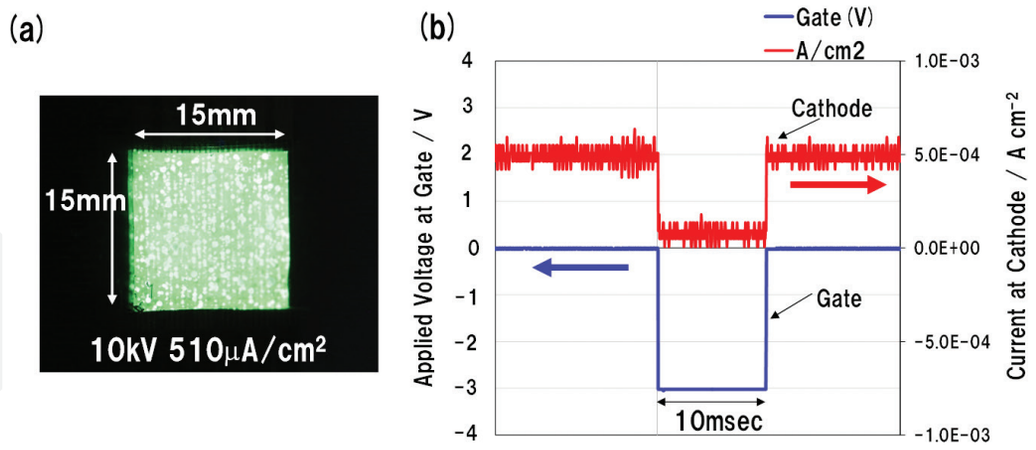

Figure 23. (a) Flat-panel light emission driven by line-sequential scanning (shaded by ND filter) [32]. (b) On-and-off chart for voltage applied to gate electrode and current flowing through cathode [32]. Copyright (2017) The Japan Society of Applied Physics.

We succeeded in assembling an FE planer electron-emission source pattern via a line-sequential-scanning method with an optimized design that the individual gate electrodes driven with an on/off FE current flowing. This was accomplished while conserving energy in cathode electrodes activated by making up scratching to emit electrons more effectively from the cathodic electrode employing a highly crystalline SWCNT. We also succeeded in amplifying the luminance-output by combining long-afterglow and high-luminance phosphors for an anode electrode to overlap the afterglow component of fluorescent materials to establish a basic design for assembling a triode flat-panel light-emission device with a line scanning sequential method. To the best of our knowledge, the creation of a flat-panel light-emission device that could achieve to obtain a high brightness efficiency of 87 lm/W was a remarkable outcome for the first time ever. Improvements to the driving performance for electron emissions at FE sources largely depend on the application of the highly crystalline SWCNTs. We believe this achievement assumes a leading role in electronic device creation through the effective use of a highly crystalline SWCNT, and we confidently need to promote its industrial design for practical use.

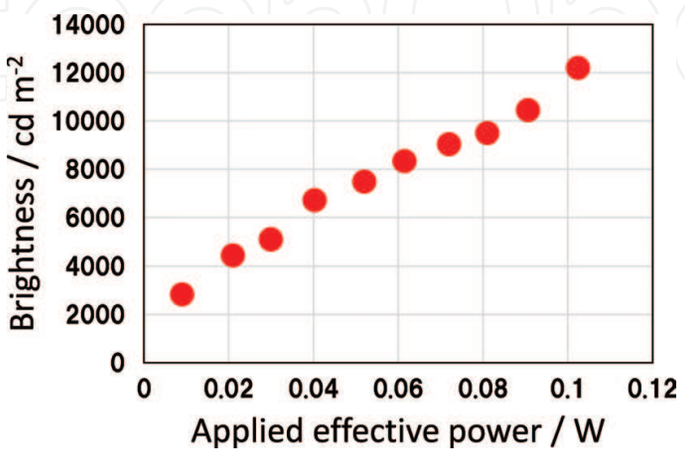

Figure 24. Relationship between power consumption and output luminance of triode flat-panel light-emission device [32]. Copyright (2017) The Japan Society of Applied Physics.

7. Conclusion

The attempt to apply highly crystalline SWCNTs as electron emission source was successfully achieved to obtain a planar light-emission device with low power consumption. Highly crystalline SWCNTs are an electrical element that can make a significant improvement in FE characteristics. A thin cathodic electrode film assembled via a wet process employing a highly crystalline SWCNT is expected to provide energy conservation as an FE electron emission source. By combining such elemental technologies both of the control the on-and-off switching of electron emissions in an arbitrary manner and the amplification of the luminance output with the persistence characteristics of a fluorescent screen, a flat-panel light-emission device with high brightness efficiency with an energy conserve driving method was assembled for the first time in the world.

The application of FE electron sources employing highly crystalline SWCNTs was determined to be effective for conserving energy based on such results, and is expected to establish other devices that are driven with low-power consumption in the future.

Acknowledgements

This work was partially supported by DOWA Holdings Co. Ltd. The author thanks the co-researchers from DOWA for their discussions and suggestions.

Author details

Norihiro Shimoi

Address all correspondence to: norihiro.shimoi.c8@tohoku.ac.jp

Graduate School of Environmental Studies, Tohoku University, Sendai, Japan

References

[1] Hamada N, Sawada S, Oshiyama A. New one-dimensional conductors: Graphitic microtubules. Physical Review Letters. 1992;**68**:1579-1581

[2] Saito R, Fujita M, Dresselhaus G, Dresselhaus MS. Electronic structure of chiral graphene tubules. Applied Physics Letters. 1992;**60**:2204-2206

[3] Tanaka K, Okahara K, Okada M, Yamabe T. Electronic properties of bucky-tube model. Chemical Physics Letters. 1992;**191**(5):469-472

[4] Kim J-Y, Kim M, Kim HM, Joo J, Choi J-H. Electrical and optical studies of organic light emitting devices using SWCNTs-polymer nanocomposites. Optical Materials. 2002; **21**:147-151

[5] Ebbesen TW, Lezec HJ, Hiura H, Bennett JW, Ghaemi HF, Thio T. Electrical conductivity of individual carbon nanotubes. Nature. 1997;**382**:54-56

[6] Wildoerm JWG, Venema LC, Rinzler AG, Smalley RE, Dekker C. Electronic structure of atomically resolved carbon nanotubes. Nature. 1998;**391**:59-62

[7] Odom TW, Huang JL, Kim P, Lieber CM. Atomic structure and electronic properties of single-walled carbon nanotubes. Nature. 1998;**391**:62-64

[8] Treacy MMJ, Ebbesen TW, Gibson JM. Exceptionally high Young's modulus observed for individual carbon nanotubes. Nature. 1996;**381**:678-680

[9] Saito Y, Uemura S, Hamaguchi K. Cathode ray tube lighting elements with carbon nanotube field emitters. Japanese Journal of Applied Physics. 1998;**37**:L346-L348

[10] Dai H, Hafner JH, Rinzler AG, Colbert DT, Smalley RE. Nanotubes as nanoprobes in scanning probe microscopy. Nature. 1996;**384**:147-150

[11] Dillon AC, Jones KM, Bekkedahl TA, Kiang CH, Bethune DS, Haben MJ. Storage of hydrogen in single-walled carbon nanotubes. Nature. 1997;**386**:377-379

[12] Niu C, Sichel EK, Hoch R, Moy D, Tennent H. High power electrochemical capacitors based on carbon nanotube electrodes. Applied Physics Letters. 1997;**70**:1480-1482

[13] Rinzler AG, Hafner JH, Nikolaev P, Lou L, Kim SG, Tomanek D, et al. Unraveling nanotubes: Field emission from an atomic nanowire. Science. 1995;**269**:1550-1553

[14] De Heer WA, Chatelain A, Ugarte D. A carbon nanotube field emission source. Science. 1995;**270**:1179-1180

[15] Collins PG, Zettl A. A simple and robust electron beam source from carbon nanotubes. Applied Physics Letters. 1996;**69**:1969-1971

[16] Saito Y, Hamaguchi K, Hata K, Uchida K, Tasaka Y, Ikazaki F, et al. Conical beams from open-ended nanotubes. Nature. 1997;**389**:554-555

[17] Bonard JM, Maier F, Stoeckli T, Chatelain A, De WA, Salvetat JP, et al. Field emission properties of multiwalled carbon nanotubes. Ultramicroscopy. 1998;**73**:7-15

[18] Fransen MJ, van Rooy TL, Kruit P. Field emission energy distributions from individual multiwalled carbon nanotubes. Applied Surface Science. 1999;**146**:312-327

[19] Saito Y, Hamaguchi K, Nishino T, Hata K, Tohji K, Kasuya A, et al. Field emission patterns from single-walled carbon nanotubes. Japanese Journal of Applied Physics. 1997;**36**:L1340-L1342

[20] Ren ZF, Huang ZP, Xu JW, Wang JH, Bush P, Siegal MP, et al. Synthesis of large arrays of well-aligned carbon nanotubes. Science. 1998;**282**:1105-1107

[21] Tsai SH, Chao CW, Lee CL, Shih HC. Bias-enhanced nucleation and growth of the aligned carbon nanotubes with open ends under microwave plasma synthesis. Applied Physics Letters. 1999;**74**:3462-3464

[22] Kim JM, Choi WB, Lee NS, Jung JE. Field emission from carbon nanotubes for displays. Diamond and Related Materials. 2000;**9**:1184-1189

[23] Iwata S, Sato Y, Nakai K, Ogura S, Okano T, Namura M, et al. Novel method to evaluate the carbon network of single-walled carbon nanotubes by hydrogen physisorption. Journal of Physical Chemistry Letters. 2007;**111**:14937-14941

[24] Shimoi N. Effect of increased crystallinity of single-walled carbon nanotubes used as field emitters on their electrical properties. Journal of Applied Physics. 2015;**118**:214304

[25] Shimoi N, Adriana LE, Tanaka Y, et al. Properties of a field emission lighting plane employing highly crystalline single-walled carbon nanotubes fabricated by simple processes. Carbon. 2013;**65**:228-235

[26] Popov VN. Carbon nanotubes: Properties and application. Materials Science & Engineering R: Reports. 2004;**43**(3):61-102

[27] Fransen MJ, van Rooy TL, Kruit P. Field emission energy distributions from individual multiwalled carbon nanotubes. Applied Surface Science. 1999;**146**:312-327

[28] Nilsson L, Groening O, Emmenegger C, Kuettel O, Schaller E, Schlapbach L. Scanning field emission from patterned carbon nanotube films. Applied Physics Letters. 2000; **76**:2071-2073

[29] Tohji K, Goto T, Takahashi H, et al. Purifying single-walled nanotubes. Nature. 1996; **383**(6602):679-679

[30] Anantram MP, Leonard F. Physics of carbon nanotube electronic devices. Reports on Progress in Physics. 2006;**69**(3):507-561

[31] Garrido SB, Shimoi N, Abe D, Hojo T, Tanaka Y, Tohji K. Plannar light source using a phosphor screen with single-walled carbon nanotubes as field emitters. Review of Scientific Instruments. 2014;**85**:104704

[32] Shimoi N, Abe D, Matsumoto K, Sato Y, Tohji K. Low-power-consumption flat-panel light-emitting device driven by field-emission electron source using high-crystallinity single-walled carbon nanotubes. Japanese Journal of Applied Physics. 2017;**56**:065101

[33] Murata H, Shimoyama H, Ohye T. Computer simulation of electric field analysis for vertically aligned carbon nanotubes: I. Simulation method and computing model. Proceedings of SPIE. 2001;**4510**:156-162

[34] Shimoyama H, Murata H, Ohye T. Computer simulation of electric field analysis for vertically aligned carbon nanotubes: II. Electric field on the nanotube apex. Proceedings of SPIE. 2001;**4510**:163-171

[35] Shimoi N, Tanaka S-I. Numerically optimized bundle size and distribution of carbon nanofibers for a field emitter. Carbon. 2010;**48**:905-911

[36] Thostenson ET, Ren ZF, Chou TW. Advances in the science and technology of carbon nanotubes and their composites: a review. Composites Science and Technology. 2001; **61**:1899-1912

IntechOpen